International Journal of Biological Macromolecules
http://dx.doi.org/10.1016/j.ijbiomac.2014.07.050

# Micro- and nano-hydroxyapatite as active reinforcement for soft biocomposites

F. Munarin[1], P. Petrini[1*], R. Gentilini[1], R. S. Pillai[2], S.Dirè[2], M.C. Tanzi[1], V.M. Sglavo[2]

[1] Laboratorio di Biomateriali, Dipartimento di Chimica, Materiali e Ingegneria Chimica 'G. Natta' and Unità di Ricerca Consorzio INSTM, Politecnico di Milano, Piazza L. da Vinci, 32- 20133 Milano, Italy

[2] Dipartimento di Ingegneria Industriali, Unità di Ricerca INSTM, Dipartimento di Ingegneria Industriale, Università di Trento, Via Sommarive 9, 38123 Trento, Italy

* Corresponding author: Paola Petrini

Laboratorio di Biomateriali, Dipartimento di Chimica, Materiali e Ingegneria Chimica 'G. Natta' and Unità di Ricerca Consorzio INSTM, Politecnico di Milano, Piazza L. da Vinci, 32- 20133 Milano, Italy

email paola.petrini@polimi.it , tel. +39 0223993386, fax +39 0223993360

## Abstract

Pectin-based biocomposite hydrogels were produced by internal gelation, using different hydroxyapatite (HA) powders from commercial source or synthesized by the wet chemical method. HA possesses the double functionality of cross-linking agent and inorganic reinforcement. The mineralogical composition, grain size, specific surface area and microstructure of the hydroxyapatite powders are shown to strongly influence the properties of the biocomposites. Specifically, the grain size and specific surface area of the HA powders are strictly correlated to the gelling time and rheological properties of the hydrogels at room temperature. Pectin pH is also significant for the formation of ionic cross-links and therefore for the hydrogels stability at higher temperatures.

The obtained results point out that micrometric-size hydroxyapatite can be proposed for applications which require rapid gelling kinetics and improved mechanical properties; conversely the nanometric hydroxyapatite synthesized in the present work seems the best choice to obtain homogeneous hydrogels with more easily controlled gelling kinetics.

*Keywords: Biocomposites, pectin, hydroxyapatite, hydrogels*

## 1. Introduction

In the last decade, biocomposite hydrogels, i.e. composite biomaterials made of an organic polymeric matrix and an inorganic reinforcement, have been developed to be used as scaffolds or delivery systems in tissue engineering.

Tissue engineering aims to heal damaged tissues by the use of implantable or injectable systems able to release bioactive agents, such as drugs, proteins, genes or cells, as well as to guide and support the regeneration of the host tissues [1-4]. Hydrogels represent a versatile class of biomaterials with attractive properties for tissue engineering, including biocompatibility, controlled biodegradability and easy manufacturing of the constructs in desired shapes [5,6].

Biocomposites have been proposed for tissue engineering either to improve the mechanical performances of the hydrogels [7,8] or to mimic specific biological structures, such as bone [9,10].

Natural polymers have an advantageous role in the production of the biocomposites, as they derive from or mimic the native extracellular matrix secreted by the cells. Among these polymers, collagen, chitosan and alginate are the typical biomaterials employed to produce natural-based biocomposites [9-17].

Concerning the inorganic reinforcing phase, tricalcium phospate and hydroxyapatite have been widely employed as reinforcement, due to their bioactive and osteoconductive properties [18-23]. The size of the inorganic reinforcement phase have a central role in the determination of the final properties of the biocomposite [24]. In particular, nano-sized fillers can drastically improve the properties of the conventional micrometric biocomposites, due to higher surface/volume ratio, better dispersion and the possibility of incorporating smaller amounts of fillers in the polymeric matrix [25,26].

Since the natural bone is composed by nano-sized hydroxyapatite crystals with needle-like morphology, several research groups synthesized and employed hydroxyapatite with a bone-like nanometric scale [27-30].

In some cases, micro-structured hydroxyapatite spheres and particles were used to improve the mechanical properties of the biocomposites [13,31,32].

In this context, the present work concerns the preparation and characterization of a novel biocomposite made of pectin and hydroxyapatite. Pectin is a natural polysaccharide showing appealing properties for biomedical applications. In recent works [33-36], it was exploited especially for cell immobilization, due to good biocompatibility and to the possibility of forming hydrogels without the use of harmful reagents.

Pectin can form gels in the presence of calcium ions [33-38]; therefore, hydroxyapatite was selected both as cross-linking agent and as reinforcement of the biocomposite. The limited water solubility of hydroxyapatite leads to obtain a soluble fraction, with free calcium ions involved in the gelling process, and an insoluble part that may act as reinforcement of the biocomposite.

The use of hydroxyapatite as a reactive compound in the polymeric matrix, in addition of being a mere reinforcement phase, is a promising strategy that can improve the connection and the permanence of the inorganic phase in the polymeric matrix, which is a critical issue to obtain stable biocomposites.

The aim of this work is to evaluate how the properties of pectin hydrogels are affected by the chemical composition, granulometry, particle aggregation, surface area and possible presence of impurities of the hydroxyapatite powders. The investigation of such parameters is carried out to gain a specific control over the gelling kinetics, pH and rheological properties of the biocomposite hydrogels, to tailor the specific requirements of tissue engineering and regenerative medicine applications.

## 2. Materials and methods

### 2.1 Materials

Three different hydroxyapatite powders were considered in the present work as inorganic second phase to be added to the organic pectin matrix. The first powder, labeled as M-HA, was provided by Eurocoating SpA (Italy) nominally consisting of pure hydroxyapatite granules, in the range 20-40 μm; the second, labeled as m-HA, was acquired by Fluidinova SA (Portugal) (nanoXIM Hap201, 2.5 μm; crystalline phase: pure hydroxyapatite; chemical analysis: Ca/P ratio = 1.66-1.72; particle size: $d_{0.1}$ = 1.4 μm, $d_{0.5}$ = 2.2 μm, $d_{0.9}$ = 3.6); the third one, labeled as n-HA, was synthesized by wet chemical method starting from reagent grade chemicals (calcium hydroxide, orthophosphoric acid, ammonium hydroxide) purchased from Sigma Aldrich.

Pectin CU701 lot 250 was kindly provided by Herbstreith & Fox (Neuemberg, Germany) and was used as received.

## 2.2 Synthesis and characterization of n-HA powder

Ammonium hydroxide solution (30 wt%) was slowly added to 240 ml of $H_3PO_4$ solution (0.25 M, pH = 1.67), until reaching pH = 8.5. Then, 100 ml of a milky $Ca(OH)_2$ suspension (prepared adding 20 g of $Ca(OH)_2$ to 0.500 l of bidistilled water) was dropped into the solution, checking continuously the pH, which reached a final value of 8.88. The white suspension was maintained under vigorous stirring overnight; then, the suspension was aged at 25°C for 24 h and at 75°C for further 24 h. After filtration, the white powders were washed several times with distilled water and dried at 75°C for 24 h. At this stage, the powder was named "as prepared" or n-$HA_{(RT)}$. After drying, n-$HA_{(RT)}$ powder was calcined in air at 650°C (heating rate = 10°C/min) for 30 min and the material was further labeled as n-$HA_{(650°C)}$.

The synthesized n-$HA_{(RT)}$ and n-$HA_{(650°C)}$ powders were subjected to physical and microstructural characterization by using complementary techniques.

The powder morphology was observed by Jeol JSM 5500 Scanning Electron Microscope (SEM), operating at 20 kV.

The synthesized powders, n-$HA_{(RT)}$ and n-$HA_{(650°C)}$, were analyzed also by Transmission Electron Microscopy (TEM) (Philips, CM12). In this case the powder was mixed with ethanol and a drop of the suspension (100 µl) was dripped over the sample holder.

XRD analysis was performed on a Rigaku D Max powder diffractometer, in Bragg-Brentano configuration, using Cu Kα radiation, in the range $2\Theta = 10°-60°$, with step 0.05° and 5 s counting time.

The chemical analysis was carried out by Inductively Coupled Plasma–Atomic Emission Spectroscopy (ICP–AES), using a Spectro Ciros instrument. The sample

was dissolved into 5 wt% $HNO_3$ solution and the measurement was repeated three times. Sigma Aldrich pure 99.99% hydroxyapatite standard and Fluka multi-element standard - sol.IV were used for the quantitative analysis of Ca - P and for the other chemical elements, respectively.

For a better comparison of the three HA powders used in the present work, also M-HA and m-HA powders were subjected to SEM, XRD and ICP characterization, using the same procedures described for the n-HA powder.

FT-IR spectra were recorded on a Thermo Optics Avatar 330 instrument, in transmission mode in the range 4000 - 400 $cm^{-1}$ using KBr pellets (64 scans, 4 $cm^{-1}$ resolution).

Solid state NMR analyses were carried out with a Bruker 300WB instrument applying a carrier frequency of 300.13MHz ($^1H$). Powder samples were packed in 4 mm zirconia rotors, which were spun at 9.5 kHz. $^{31}P$ SP MAS spectra were recorded at 121.49 MHz, with a $\pi/2$ pulse length of 3.6 μs and proton decoupling, recycle delay 300 s, acquiring 16 scans. The CP MAS experiment was run with contact time of 5 ms, recording 100 scans. Ammonium dihydrogen phosphate $(NH_4)H_2PO_4$ was used as secondary reference. $^1H$ MAS spectra were performed at 300.13 MHz, 5 μs $\pi/2$ pulse length, recycle delay 5 s, averaging 16 scans. Ethanol was used as secondary reference.

$N_2$-physisorption measurements were performed with a Micromeritics ASAP 2010 instrument. The samples were degassed below 1.3 Pa prior to the analysis. The Specific Surface Area (SSA) of the samples was evaluated with the BET equation within the relative pressure range: $0.05 \leq P/P_0 \leq 0.33$. BJH model was used for calculating the pore size distribution.

### 2.3 Preparation and characterization of the composite gels

HA-containing pectin composites were prepared by mixing pectin solutions at pH 3.2 ±0.1 (native pH) and pH 3.7±0.1 (adjusted with 5M NaOH) with 0.1% (w/v) hydroxyapatite suspensions, obtaining a final 3% (w/v) pectin concentration. Pectin composites were produced with M-HA, m-HA, n-$HA_{(RT)}$ and n-$HA_{(650°C)}$ hydroxyapatite powders. The samples were obtained in cylindrical molds (⦸ = 2 cm) and were characterized 24 h after preparation.

The pH of the produced hydrogels was measured using a Cyberscan pH 110219 pHmeter (Eutech Instruments) with a penetration electrode (Hamilton double pore slim) specific for soft gels.

After preparation, hydrogels were dried in the oven (T = 37° C), then frozen with nitrogen, ground in a mortar and embedded in KBr pellets. FT-IR analysis was performed as described for n-HA powder characterization.

Rheological analysis was carried out with an AR 1500ex rheometer (TA Instruments, Italy), equipped with parallel-plate geometry (diameter = 20 mm, working gap = 1000 μm). Time sweep test (σ = 5 Pa, F = 0.7 Hz, T = 25°C) was assessed to measure the gel point, i.e. the time at which the transition from viscous solution to solid-like gel is reached and, therefore, to evaluate the gelling kinetics of the different formulations. Oscillatory analysis was set up to investigate the evolution of storage (G') and loss modulus (G") with strain (oscillation amplitude tests, T = 25°C, f = 1 Hz, strain = 1-100%) and frequency (frequency sweep tests, T = 25°C, f = 0.1-10 Hz, strain = 1%). Temperature ramps were performed in oscillatory mode increasing the test temperature from 20°C to 50 °C (ramp rate = 2.5°C/min), to simulate the behavior of pectin hydrogels when subjected to physiological and storage temperatures.

## 3. RESULTS

### 3.1 Physical and chemical properties of the HA powders

Figure 1 shows the morphology (SEM micrographs) of the HA powders considered in the present work. M-HA powder corresponds to large spherical granules from about 2 μm to 40 μm diameter (Figure 1a); each granule is constituted of a multitude of strongly bonded small grains of about 1-2 μm. m-HA powder is composed by spherical structures with size ranging from 0.1-0.2 μm to 4 μm although their consistence appears less dense than in M-HA sample (Figure 1b). n-HA powder (both as prepared and calcined at 650°C) appears as randomly shaped flocs formed by the weak interactions of nanometric-size particles (Figure 1c-d).

The morphology of the synthesized n-HA powder (as-produced and calcined at 650°C) is shown in the TEM micrograph reported in Figure 2, where isometric single grain particles are clearly visible. The dimension of the calcined powder is slightly larger and the complete particles size distribution of the sample, as determined by direct measurement on TEM micrographs is shown in Figure 3: an average grain size of about 25 nm was therefore determined, more than 90% of the particles being included in the 10-45 nm interval. Unfortunately, the strongly agglomerated structure of the as-produced powder impeded the measurement of the distribution. Nevertheless, from Figure 2a one can estimate an average size for the as-synthesized n-HA powder slightly lower than 25 nm.

The XRD diagrams recorded on the powders considered in the present work are shown in Figure 4. The diffraction peaks correspond to pure hydroxyapatite ($Ca_5(PO_4)_3OH$ - JCPDS No: 09-0432) although the relative intensity and peak width changes among the samples. In particular, the limited intensity and broadness of

signals recorded on m-HA and n-HA samples are an indication of their nanocrystalline nature; as a matter of fact, by using the Sherrer's equation [39] considering the well resolved peak at about 25.9°, an average crystallite size equal to 16 nm and 23 nm was estimated for as-prepared and calcined n-HA powder, respectively. The estimated value is therefore in very good agreement with TEM observations (Figure 2). Similar values (16 nm crystallite size) were obtained for m-HA powder, this pointing out that the spherical structures shown in Figure 1 correspond to relatively big agglomerates of nanometric powders. Quite surprisingly, the same calculation performed on M-HA powder lead to an average crystallite size estimate of about 60 nm; this indicate that the single grains constituting the granules observed in SEM micrographs (Figure 1a) are themselves composed by nanocristalline grains.

The chemical analysis performed on n-HA powder by ICP-AES revealed the presence of Ca and P and the absence of any other metal; the Ca/P ratio is equal to 1.649 and 1.668 (estimated error = 0.012) for as-synthesized and calcined n-HA powder, respectively, in good agreement with the stoichiometric ratio for pure HA equal to 1.667. Similar results were obtained from the chemical analysis of M-HA and m-HA powders whose Ca/P ratio determined by ICP is equal to 1.670 and 1.660, respectively.

FTIR spectra of as-prepared and calcined n-HA powders are shown in Figure 5. The as-prepared powder shows the signals associated with the characteristic vibrations of phosphates and -OH groups in HA crystal lattice [40]. However, the increase in cristallinity is observable after the thermal treatment at 650°C (Figure 2b). The $PO_4^{3-}$ groups show the typical signals at 1095 and 1053 $cm^{-1}$ (ν3, broad), 961 $cm^{-1}$ (ν1), 602 and 571 $cm^{-1}$ (ν4, sharp) and at 475 $cm^{-1}$ (ν2). The -OH stretching and bending

vibrations are found at 3570 and 628 $cm^{-1}$, respectively. The very weak signals in the range 2200 - 1900 $cm^{-1}$ are assigned to surface P-OH vibration modes [41]. The stretching and bending vibration signals of adsorbed water (3435 and 1630 $cm^{-1}$) are present in both spectra of Figure 2b. The doublet at 1466 and 1411 $cm^{-1}$ is frequently found for HA powders prepared by wet chemistry, and it is attributed to $CO_3^{2-}$ groups formed as a consequence of $CO_2$ dissolution from air into the solutions [42]. Moreover, the carbonate phase could also derive from the $Ca(OH)_2$ transformation in air. As a matter of fact, in the spectrum of n-HA treated at 650 °C, two very small signals at 3640 and 875 $cm^{-1}$ account for the presence of residual calcium hydroxide [43] whose presence is attributed in the literature to the reaction of CaO with moisture.

The FTIR spectra of m-HA and M-HA powders show the typical HA vibrations found in n-HA spectra (Figure 5b). The broadness of the phosphate band in M-HA, in the range 1500-700 $cm^{-1}$, is noteworthy and a carbonate phase is detected in m-HA (Figure 5b).

In addition to vibrational spectroscopy, solid state NMR has been employed to study n-HA powders, with the aim of characterizing P and H nuclei local environment and detecting the presence of different phases, particularly amorphous ones. $^{31}P$ SP MAS NMR spectra are characterized by a sharp peak and a very broad and weak low-field resonance, overlapped to the main signal. This evidence is particularly clear if one observes the corresponding CP MAS spectra (Figure 6a). By deconvolution of the SP MAS spectrum of the as-prepared sample (confidence 95%), three components are found: a main signal at 3.2 ppm (83%) assigned to crystalline HA; a resonance at 3.9 ppm (11 %), which could be attributed to poorly crystallized hydroxyapatite; a small component at 5.6 ppm (6 %) that could be assigned to a different calcium phosphate

phase like not stoichiometric HA or TCP [44-46]. The sample treated at 650 °C shows a significant signal narrowing, suggesting an increase in crystallinity, and the strong reduction (0.7 %) of the signal at 5.6 ppm.

The proton spectra (Figure 6b) are quite resolved and present sharp peaks, with the exception of the broad water resonance at 4.9 ppm. The spectra deconvolution (confidence 95%) allows to recognize the main component at -0.5 ppm, due to OH in HA crystal lattice [47]. Moreover, two small sharp peaks are also detected at lower fields (1.0 and 1.8 ppm) and probably account for mobile OH belonging to surface adsorbed water. Indeed, Pourpoint et al. [48] found up to four water -OH resonances in similar materials.

The textural features of the nanometric powders have been studied by $N_2$ physisorption, collecting adsorption-desorption isotherms on as-prepared and heat treated powders (Figure 7a-b).

As-prepared powder is characterized by a type IIb isotherm typical of meso- and macro-porous materials with H3-type hysteresis loop without plateau at high pressure, indicating the presence of plate like particles [49]. The relevant results calculated from $N_2$ isotherms are reported in Table 1. As-prepared powders show high specific surface area (SSA) and total porosity (TPV) with a broad pore size distribution in the meso- macro-pores region (Figure 7c). The pore size distribution obtained from the desorption branch appears shifted towards smaller pore diameters, probably in relation with the presence of ink-bottle pores rather than perfectly cylindrical ones.

SSA and TPV values decrease as a consequence of the thermal treatment but with unchanged features, as it can be deduced from the isotherm trace (Figure 7b). A further broadening of pore size distribution is observed after the thermal treatment with the increase of larger pores amount (Figure 7d).

m-HA powders present high SSA and TPV values (Table 1) and a pore size distribution similar to that displayed by as-prepared n-HA powders. On the contrary M-HA sample is characterized by very low porosity.

Finally, ICP analysis was performed on the hydroxyapatite powders suspended at different pH to study the dissolution of calcium and phosphates ions during the dispersion of the powders in water (pH 7) or HCl solutions at pH 3.2 and 3.7.

The increase of Ca and P dissolution was related to the decrease of the solution pH (Figure 8) but a clear dependence on the duration of the incubation could not be identified: the dissolution of Ca and P after 10 minutes of incubation resulted comparable to the one measured after 24 of incubation in the same acidic solvent (Figure 8).

### 3.2 Preparation of the composite hydrogels and pH variations

Composites hydrogels were produced using 3% (w/v) pectin and 0.1% (w/v) M-HA, m-HA, n-$HA_{(RT)}$ and n-$HA_{(650°C)}$ hydroxyapatite powders. The properties of pectin hydrogels are known to be easily tunable by varying the pH of pectin solutions [37] and the solubility of hydroxyapatite is strongly dependent on pH, thus modifying the amount of $Ca^{2+}$ available for the crosslinking. Hydrogel samples were produced at different pH, employing pectin at its native pH (pH 3.2) or adjusting the pH to 3.7.

As shown in previous works [37], the cross-linking promotes an increase of pH for each formulations, due to the complexation of the pectin carboxylic groups by calcium ions released by hydroxyapatite. No significant trends could be seen for the pH of hydrogels prepared with pectin at pH 3.2, whose pH increase by 0.2 ± 0.1 after cross-linking, independently upon the typology of hydroxyapatite employed (Table 2). Conversely, when using pectin at pH 3.7, Pect m-HA hydrogels showed the

highest pH after cross-linking (Table 2), while the pH of the hydrogels produced with M-HA and n-HA showed slight variations.

The gel point was measured with a time-sweep rheological test, and it is shown in Table 2 as the time at which the crossover of the storage and loss modulus occurs.

The hydrogels prepared with pectin at native pH (pH 3.2) showed fast gelling kinetics, reaching the gel point in less than 4 min. The gel point of the hydrogels produced using pectin at pH 3.7 depends upon the specific hydroxyapatite powder, this effect being probably related to the different solubility rate associated with the different microstructure. While m-HA hydrogels at pH 3.7 exhibited a fast gelling kinetic ($t_{gel\ point}$ < 4 min) comparable to that of the native pectin, M-HA hydrogels showed the longest crosslinking time, as the formation of a solid- like gel structure was obtained more than 60 min after the preparation (Table 2). n-$HA_{(RT)}$ and n-$HA_{(650°C)}$ powders allowed reaching the gel point in 5 and 8 min, respectively. This slight difference compared to m-HA might be attributed to the powders composition and, more specifically, to the presence of calcium carbonate and calcium hydroxide groups in n-$HA_{(RT)}$ and, in minor amounts, in n-$HA_{(650°C)}$ samples (Figure 5a).

Some exemplary micrographs of the dried hydrogels acquired at SEM show the good dispersion of the hydroxyapatite powders in Pect M-HA and Pect m-HA samples (Figure 9a-b), and the formation of aggregates in Pect n-$HA_{(650°C)}$ hydrogels (Figure 9c).

### 3.3 Characterization of the composite hydrogels

Pectin-hydroxyapatite composite hydrogels were analyzed by FT-IR spectroscopy in the spectral area of 2000-400 $cm^{-1}$ (Figure 10) to detect the structural characteristics of the hydrogels. Stretching and bending modes of $PO_4^{3-}$ appeared at 602 $cm^{-1}$ and

571 $cm^{-1}$ in the IR spectra of pectin – hydroxyapatite hydrogels. Furthermore, the spectral bands at 961 $cm^{-1}$, attributed to symmetric ν1 P-O stretching, and at 1095 $cm^{-1}$ and 1053 $cm^{-1}$, attributed to asymmetric ν3 P–O stretching modes of the phosphate groups, were visible.

Comparing the spectra of the dried hydrogels with the one of pectin powders, the broad bands appearing at 1420 $cm^{-1}$, as well as the relative variations of intensity of peaks at 1745 and 1625 $cm^{-1}$ suggest the cross-linking of pectin and calcium ions from hydroxyapatite. In particular, the decrease in intensity of the peak at 1745 $cm^{-1}$, associated to the C=O stretching vibrations of the carboxyl groups can account for the formation of ionic interactions. Accordingly, the significant increase of the bands at 1625 $cm^{-1}$ and 1420 $cm^{-1}$ can be related to the presence of ionized $COO^-$ groups in pectin backbone due to the salification of COOH groups, thus indicating gel formation.

When pectin is treated with NaOH to increase the pH, the degree of esterification (DE) is known to decrease [50]. The bands associated to DE variations (between 1745 $cm^{-1}$ and 1625 $cm^{-1}$) are the same or in the same spectral regions of the bands involved in the cross-linking (COOH groups at 1745 $cm^{-1}$ and $COO^-$ groups at 1625 $cm^{-1}$). Comparing the peak areas of hydrogels at pH 3.2 and pH 3.7, evidences about the decrease of DE can be detected. The decrease of stretching of the carbonyl in the ester bond (at 1745 $cm^{-1}$), associated to the increase of the carboxylate (1625 $cm^{-1}$ and 1420 $cm^{-1}$) of hydrogels at pH 3.7 may suggest pectin de-esterification as a consequence of the treatment with sodium hydroxide (Table 3).

As shown in Table 3, the highest (COOH+COO-R)/$COO^-$ ratio is measured for pectin powders, where, in the absence of the cross-linker, the very strong IR band at 1745

$cm^{-1}$ can be attributed to the C=O stretching of the undissociated COOH and $COOCH_3$ groups.

As a consequence of the cross-linking of pectin at its native pH (pH=3.2), the reduced (COOH+COO-R)/$COO^-$ ratio is caused by the increase of the 1625 $cm^{-1}$ and 1420 $cm^{-1}$ peak areas, due to the ionic complexation of pectin carboxyl groups with calcium ions derived from hydroxyapatite. In this case, the ratio appears to be dependent upon the hydroxyapatite granulometry, being n-$HA_{(650°C)}$ the powder which provides the highest crosslinking efficiency and M-HA the lowest. This behavior might be attributed to the improved water solubility of the hydroxyapatite with the smallest granules.

Increasing the pH of pectin solutions to 3.7 prior to gelling leads to a further decrease of the (COOH+COO-R)/$COO^-$ ratio, resulting from the combination of two different contributes: the dissociation of the COOH groups of pectin chains to $COO^-$ due to the increase of pH and the ionic complexation with calcium ions released from hydroxyapatite, and the dissociation of the $COOCH_3$ groups to $COO^-$ due to de-esterification. It can be hypothesized that the contribution of COOH and $COOCH_3$ dissociation is predominant and therefore it masks the peak area increase caused by the formation of the cross-links. Thus, in this case, no evidences of correlations among the granulometry of the hydroxyapatite powders and the COO-R/$COO^-$ ratio were observed.

Rheological studies were performed to evaluate the mechanical properties of the produced hydrogels. Oscillation amplitude test showed a linear viscoelastic region in the range of 1-10% strain for all the considered samples (data not shown), therefore all the experiments further performed were conducted in this strain range.

Pectin-hydroxyapatite composite hydrogels showed a frequency-dependent behavior, slightly increasing the storage and loss moduli and decreasing the complex viscosity with frequency (Figure 11). For each sample, the gels prepared employing native pectin (pH = 3.2) appeared thicker than those prepared using pectin with higher pH (pH=3.7). Generally, the use of m-HA resulted in the production of the thickest formulations while n-HA powders, appositely produced for this study, showed intermediate rheological properties in terms of storage modulus and complex viscosity (Figure 11a-b). Furthermore, the use of calcined n-$HA_{(650°C)}$ powders led to obtain softer pectin hydrogels with respect of n-$HA_{(RT)}$ (Figure 11c).

The storage and loss moduli of the pectin – hydroxyapatite hydrogels were found to decrease when increasing the test temperature (Figure 12): while a slight decrease can be observed for the hydrogels produced with pectin at pH 3.7, a significant loss of the storage modulus was detected for the samples prepared with pectin at its native pH. According to the results of the frequency sweep tests, n-$HA_{(RT)}$ showed higher storage modulus than n-$HA_{(650°C)}$ in the temperature ramp test (Figure 12b).

## 4. Discussion

In this work, different hydroxyapatite powders, supplied or custom-produced, were characterized with the final aim to control the resulting properties of the biocomposite soft hydrogels. The powders under investigation showed differences in terms of composition, grain size, porosity and solubility (Figures 1-8).

Hydroxyapatite was employed to produce pectin composite hydrogels via internal gelation, using it either as source of $Ca^{2+}$ ions and as reinforcement of the polymeric matrix. The final properties of pectin-hydroxyapatite hydrogels were deeply affected by the typology of the inorganic phase. The use of hydroxyapatite with high specific

surface area, total porosity, pore size and solubility (m-HA and n-$HA_{(RT)}$) led to the formation of thicker gels, as evaluated by rheology, and higher pH.

The solubility of hydroxyapatite powders however was strictly related to the gelling kinetics of pectin hydrogels: the rapid dissolution of the $Ca^{2+}$ ions from the hydroxyapatite powders led to a fast cross-linking of the carboxylic groups of pectin (Table 2 and Figure 8). n-HA powders showed the best compromise regarding the gelling kinetics: 5 to 8 minutes is indeed slow enough to obtain a uniform dispersion of the hydroxyapatite in the organic matrix and, therefore, a homogeneous hydrogel, but fast enough to prevent the precipitation of the insoluble hydroxyapatite fraction. In view of the final application, i.e. tissue engineering, a gelling time of 5-10 minutes is convenient as it provides the possibility to immobilize in the hydrogel the drugs or cells to be used as therapeutic agents prior to gelling.

Though in the literature micro-sized hydroxyapatite is described to improve the mechanical properties of soft hydrogels [13,31,32], in our study the granulometry of the powders did not come out to be by itself a determinant parameter for the production of thicker hydrogels. In fact, the biocomposites obtained with the 30 μm-sized hydroxyapatite (M-HA) showed lower storage modulus than the other hydrogels produced with smaller granules hydroxyapatite (m-HA and n-HA) either in the frequency either in the temperature ramp tests (Figures 11 and 12).

In this work, low amounts of hydroxyapatite were used to produce the biocomposites (0.1% w/v). Further studies are therefore needed in order to evaluate the effects of the hydoxyapatite granulometry in biocomposites with a preponderant inorganic phase. For such harder hydrogels, mainly proposed for bone regeneration [18-23], the use of n-HA powders could be preferred, in order to mimic the internal architecture of the bone.

We considered the use of pectin, as organic matrix of the composite hydrogels as it is extensively used in the food industry, but in the last decade it has also raised the interest for biomedical and biological applications, due to the encouraging results obtained in the field of tissue engineering [33-36]. The main concern in the use of such natural polymer is its acid pH, which can generate adverse reactions in the organism, including the inflammatory response. We demonstrated the possibility of producing pectin composite hydrogels at different pH, by varying the initial pH of pectin solutions and the type of hydroxyapatite (Table 2). The modulation of the pH of the hydrogels is essential to reach a compromise between the rheological parameters (viscosity, storage and loss modulus, Figures 11 and 12) and the gelling kinetics, to provide the homogeneity of the gel structure and the possible immobilization of active agents, such as cells or drugs.

On the other hand, the composites at lower pH showed higher rheological parameters but a temperature-dependent behavior (Figure 12). This effect can be explained with the change in viscosity of pectin solutions: at lower pH, pectin solutions behave like a viscoelastic solid due to the formation of entanglements and secondary bonds, such as hydrogen bonds and Van der Waals forces, while increasing the pH they assume the characteristics of a liquid. Our hypothesis is that at low pH (pH 3.2) the dissolution of the calcium ions from hydroxyapatite is improved, but the dissociation of the COOH groups of pectin chains in $COO^-$ groups, necessary for the cross-linking, is prevented. The physical interactions, i.e. hydrogen bonds and Van der Waals forces, led to obtain thicker hydrogels at room temperature, but they are disrupted when increasing the test temperature, resulting in the weakening of the hydrogels.

On the opposite, the hydrogels produced at higher pH (pH 3.7) are softer at room temperature, due to the lower amount of calcium released from hydroxyapatite, but

the COOH groups of pectin chains are dissociated in $COO^-$ groups and are prone to react with calcium ions. According to this hypothesis, these hydrogels showed a temperature-independent behavior, indicating the formation of stable cross-links.

On the overall, the produced biocomposites showed tunable physical-chemical characteristics depending on the batch of hydroxyapatite employed. According to the results of gel composition, gelling kinetics, pH and rheology, the biocomposites can be proposed as soft hydrogels for tissue engineering and regenerative medicine applications, and particularly as delivery systems such as drug or cell carriers.

## 5. Conclusions

The combination of a natural polysaccharide, i.e. pectin, with an inorganic reinforcement present in the physiological tissues, employed with the double function of curing agent and reinforcement of the biocomposites.

The physico-chemical characterization of the hydroxyapatite powders was correlated to the properties of the final biocomposite hydrogels. More in details, the chemical composition, granulometry, surface area and solubility of the hydroxyapatite powders considered in this work deeply affected the gelling kinetics, rheological properties and temperature stability of the obtained biocomposite hydrogels.

The nanometric hydroxyapatite powders produced in this work showed great potential for the development of soft hydrogels that can be proposed as cell or drug delivery systems suitable for tissue engineering applications.

## ACKNOWLEDGEMENTS

This work was supported by grants from Fondazione Cassa di Risparmio di Trento e Rovereto, SG2329/2011-2011/0206 to M.C. Tanzi and from MIUR, PRIN 2010-11

project (prot. 2010FPTBSH 009) to P. Petrini. Dr. E. Callone ("Klaus Muller" NMR Laboratory, DII, University of Trento) is gratefully acknowledged for the NMR analyses.

The authors wish to thank Eurocoating S.p.A. (Pergine Valsugana, TN, Italy) for providing the micro-sized hydroxyapatite (M-HA) used in this study.

**References**

[1] L. Lu, Y. Qi, J. Tian, C. Zhou Alginate/hydroxyapatite hydrogel as biodegradable in situ forming scaffold. 7th Asian-Pacific Conference on Medical and Biological Engineering. IFMBE Proceedings 19 (2008), pp. 22-25.

[2] T. Coradin, N. Nassif, J. Livage. Silica-alginate composites for microencapsulation. Appl Microbiol Biotechnol, 61 (2003), pp. 429-434.

[3] F. Wang, Z. Li, M. Khan, K. Tamama, P. Kuppusamy, W. R. Wagner, et al. Injectable, rapid gelling and highly flexible hydrogel composites as growth factor and cell carriers. Acta Biomaterialia, 6 (2010), pp. 1978-1991.

[4] X. Struillou, H. Boutigny, Z. Badran, B. Fellah, O. Gauthier, S. Sourice, et al. Treatment of periodontal defects in dogs using an injectable composite hydrogel/biphasic calcium phosphate. J Mater Sci Mater Med, 22 (2011), pp. 1707-1717.

[5] A.S. Hoffman. Hydrogels for biomedical applications. Adv Drug Deliv Rev, 54 (2002), pp. 3-12.

[6] D.G. Pedley, P. J. Skelly, B. J. Tighe. Hydrogels in Biomedical Applications. British Polymer Journal, 12 (1980), pp. 99-110.

[7] J. Chen, M. Tsai, H. Liao. Incorporation of biphasic calcium phosphate microparticles in injectable thermoresponsive hydrogel modulates bone cell proliferation and differentiation. Coll Surf b, 110 (2013), pp. 120-129.

[8] M. G. Raucci, V. Guarino, L. Ambrosio. Hybrid composite scaffolds prepared by sol–gel method for bone regeneration. Composite Sci Technol, 70 (2010), pp. 1861-1868

[9] F. Brun, G. Turco, A. Accardo, S. Paoletti. Automated quantitative characterization of alginate/hydroxyapatite bone tissue engineering scaffolds by

means of micro-CT image analysis. J Mater Sci Mater Med, 22 (2011), pp. 2617-2629.

[10] G. Turco, E. Marsich, F. Bellomo, S. Semeraro, I. Donati, F. Brun, et al. Alginate/Hydroxyapatite Biocomposite For Bone Ingrowth: A Trabecular Structure With High And Isotropic Connectivity. Biomacromolecules, 10 (2009), pp. 1575-1583.

[11] S. Sotome, T. Uemura, M. Kikuchi, J. Chen, S. Itoh, J. Tanaka, et al. Synthesis and in vivo evaluation of a novel hydroxyapatite/collagen–alginate as a bone filler and a drug delivery carrier of bone morphogenetic protein. Mat. Sci. Eng. C, 24 (2004), pp. 341-347.

[12] D.A. Wahl, J. T. Czernuszka. Collagen-hydroxyapatite composites for hard tissue repair. Eur Cell Mater , 11 (2006), pp. 43-56.

[13] J. Watanabe, M. Kashii, M. Hirao, K. Oka, K. Sugamoto, H. Yoshikawa, et al. Quick-forming hydroxyapatite/agarose gel composites induce bone regeneration. J Biomed Mater Res A, 83 (2007) pp. 845-852.

[14] F. De Paula, I. Barreto, M. Rocha-LeÃ£o, R. Borojevic, A. Rossi, F. Rosa, et al. Hydroxyapatite-alginate biocomposite promotes bone mineralization in different length scales *in vivo*. Front mat sci china, 3 (2009) pp. 145-153.

[15] M. Swetha, K. Sahithi, A. Moorthi, N. Srinivasan, K. Ramasamy, N. Selvamurugan. Biocomposites containing natural polymers and hydroxyapatite for bone tissue engineering. Int J Biol Macromol, 47 (2010) pp. 1-4.

[16] C. Korach, G. Halada, H. Mubarez Mechanics of Biological Systems and Materials, Volume 2. Conference Proceedings of the Society for Experimental Mechanics Series (2011), pp. 125-130.

[17] F. Khan, S. R. Ahmad. Polysaccharides and Their Derivatives for Versatile Tissue Engineering Application. Macromol Biosci, 13 (2013) pp. 395-421.

[18] S.J. Peter, S. T. Miller, G. Zhu, A. W. Yasko, A. G. Mikos. In vivo degradation of a poly(propylene fumarate)/β-tricalcium phosphate injectable composite scaffold. J Biomed Mater Res, 41 (1998) pp. 1-7.

[19] M.A. Lopes, F. J. Monteiro, J. D. Santos, A. P. Serro, B. Saramago. Hydrophobicity, surface tension, and zeta potential measurements of glass-reinforced hydroxyapatite composites. J Biomed Mater Res, 45 (1999), pp. 370-375.

[20] S.C. Rizzi, D. J. Heath, A. G. A. Coombes, N. Bock, M. Textor, S. Downes. Biodegradable polymer/hydroxyapatite composites: Surface analysis and initial attachment of human osteoblasts. J Biomed Mater Res, 55 (2001) pp. 475-486.

[21] M.S. Abu Bakar, M. H. W. Cheng, S. M. Tang, S. C. Yu, K. Liao, C. T. Tan, et al. Tensile properties, tension–tension fatigue and biological response of polyetheretherketone–hydroxyapatite composites for load-bearing orthopedic implants. Biomaterials, 24 (2003) pp. 2245-2250.

[22] M. Swetha, K. Sahithi, A. Moorthi, N. Srinivasan, K. Ramasamy, N. Selvamurugan. Biocomposites containing natural polymers and hydroxyapatite for bone tissue engineering. Int J Biol Macromol, 47 (2010) pp. 1-4.

[23] F.A. Barber, W. D. Dockery, S. A. Hrnack. Long-term degradation of a poly-lactide co-glycolide/beta-tricalcium phosphate biocomposite interference screw. Arthroscopy, 27 (2011) pp. 637-643.

[24] J. Liang. Reinforcement and quantitative description of inorganic particulate-filled polymer composites. Composites Part B: Engineering, 51 (2013) pp. 224-232.

[25] L. Avérous. Nano- and Biocomposites. Materials Today, 13 (2010) p. 57.

[26] K. Pielichowska, S. Blazewicz. Bioactive Polymer/Hydroxyapatite (Nano)composites for Bone Tissue Regeneration. Biopolymers. Advances in Polymer Science 232 (2010), pp 97-207.

[27] S. Itoh, M. Kikuchi, Y. Koyama, K. Takakuda, K. Shinomiya, J. Tanaka. Development of an artificial vertebral body using a novel biomaterial, hydroxyapatite/collagen composite. Biomaterials, 23 (2002), pp. 3919-3926.

[28] F. Chen, Z. Wang, C. Lin. Preparation and characterization of nano-sized hydroxyapatite particles and hydroxyapatite/chitosan nano-composite for use in biomedical materials. Mater Lett, 57 (2002), pp. 858-861.

[29] R. Murugan, S. Ramakrishna. Development of nanocomposites for bone grafting. Composit Sci Technol, 65 (2005), pp. 2385-2406.

[30] S. Kim, M. Sun Park, O. Jeon, C. Yong Choi, B. Kim. Poly(lactide-co-glycolide)/hydroxyapatite composite scaffolds for bone tissue engineering. Biomaterials, 27 (2006), pp. 1399-1409.

[31] W. Bonfield. Hydroxyapatite-Reinforced Polyethylene as an Analogous Material for Bone Replacement. Ann N.Y. Acad Sci, 523 (1988), pp. 173-177.

[32] N. Ignjatovic, D. Uskokovic. Synthesis and application of hydroxyapatite/polylactide composite biomaterial. Appl Surf Sci, 238 (2004), pp. 314-319.

[33] F. Munarin, P. Petrini, M. C. Tanzi, M. A. Barbosa, P. L. Granja. Biofunctional chemically modified pectin for cell delivery. Soft Matter, 8 (2012), pp. 4731-4739.

[34] F. Munarin, M. C. Tanzi, P. Petrini. Advances in biomedical applications of pectin gels. Int J Biol Macromol, 51 (2012), pp. 681-689.

[35] F. Munarin, S. S. Guerreiro, M. A. Grellier, M. C. Tanzi, M. A. Barbosa, P. Petrini, et al. Pectin-based injectable biomaterials for bone tissue engineering. Biomacromolecules, 12 (2011), pp. 568-577.

[36] F. Munarin, P. Petrini, S. Farè, M. Tanzi. Structural properties of polysaccharide-based microcapsules for soft tissue regeneration. J Mater Sci Mater Med, 21 (2010), pp. 365-375.

[37] H.R. Moreira, F. Munarin, R. Gentilini, L. Visai, P. L. Granja, M. C. Tanzi, et al. Injectable pectin hydrogels produced by internal gelation: pH dependence of gelling and rheological properties. Carbohydr Polym, 103 (2014), pp. 339-347.

[38] P. Petrini, M.C. Tanzi, L. Giuliano, F. Munarin, P. Robotti, G. Bianchi, Composite material comprising pectin and calcium phosphate and method for its realization**.** Patent n. WO/2012/007917, 19/01/2012

[39] P. Scherrer. Bestimmung der Größe und der inneren Struktur von Kolloidteilchen mittels Röntgenstrahlen. Nachrichten von der Gesellschaft der Wissenschaften zu Göttingen, Mathematisch-Physikalische Klasse, (1918) pp. 98-100.

[40] S. Zhou, X. Zheng, X. Yu, J. Wang, J. Weng, X. Li, et al. Hydrogen Bonding Interaction of Poly(d,l-Lactide)/hydroxyapatite Nanocomposites. Chem Mater, 19 (2007), pp. 247-253.

[41] L. Borum-Nicholas, O. C. Wilson Jr. Surface modification of hydroxyapatite. Part I. Dodecyl alcohol. Biomaterials, 24 (2003), pp. 3671-3679.

[42] Z.H. Cheng, A. Yasukawa, K. Kandori, T. Ishikawa. FTIR Study of Adsorption of CO2 on Nonstoichiometric Calcium Hydroxyapatite. Langmuir, 14 (1998), pp. 6681-6686.

[43] A. Ślósarczyk, C. Paluszkiewicz, M. Gawlicki, Z. Paszkiewicz. The FTIR spectroscopy and QXRD studies of calcium phosphate based materials produced from the powder precursors with different CaP ratios. Ceram Int, 23 (1997), pp. 297-304.

[44] J.L. Miquel, L. Facchini, A. P. Legrand, C. Rey, J. Lemaitre. Solid state NMR to study calcium phosphate ceramics. Coll Surf, 45(1990), pp. 427-433.
[45] S. Gomes, G. Renaudin, A. Mesbah, E. Jallot, C. Bonhomme, F. Babonneau, et al. Thorough analysis of silicon substitution in biphasic calcium phosphate bioceramics: A multi-technique study. Acta Biomaterialia, 6 (2010), pp. 3264-3274.
[46] A.P. Legrand, H. Sfihi, N. Lequeux, J. Lemaître. 31P Solid-State NMR study of the chemical setting process of a dual-paste injectable brushite cements. J Biomed Mater Res B, 91B(2009), pp. 46-54.
[47] C. Jäger, T. Welzel, W. Meyer-Zaika, M. Epple. A solid-state NMR investigation of the structure of nanocrystalline hydroxyapatite. Magn Reson Chem, 44 (2006), pp. 573-580.
[48] F. Pourpoint, C. Gervais, L. Bonhomme-Coury, T. Azaïs, C. Coelho, F. Mauri, et al. Calcium Phosphates and Hydroxyapatite: Solid-State NMR Experiments and First-Principles Calculations. Appl Magn Reson, 32 (2007), pp. 435-457.
[49] F. Rouquerol, J. Rouquerol, K. Sing Adsorption by Powders and Porous Solids. San Diego: Academic Press; 1999.
[50] C.M.G.C. Renard, J. Thibault. Degradation of pectins in alkaline conditions: kinetics of demethylation. Carbohydr Res, 286 (1996), pp. 139-150.

*Table 1. Porosity parameters calculated from $N_2$ sorption isotherms of the hydroxyapatite powders.*

| **Measured parameters** | **n-HA$_{(RT)}$** | **n-HA$_{(650\ °C)}$** | **m-HA** | **M-HA** |
|---|---|---|---|---|
| BET SSA, $m^2/g$ | 118.5 | 55.6 | 103.9 | 0.61 |
| TPV $cm^3/g$ (calculated at $P/P_0$ 0.992) | 0.532 | 0.492 | 0.468 | 0.00088 |
| Average pore diameter , Å (4V/A by BET) | 179.6 | 354.2 | 180.3 | 58.4 |
| BJH Ads Average pore diameter, Å | 171.8 | 386.8 | 172.8 | 104.1 |
| BJH Des Average pore diameter, Å | 162.5 | 333.1 | 158.6 | ------- |

*Table 2. Properties of the biocomposite hydrogels.*

| **Nomenclature** | | **Type of of HA powders** | **Gel point (min)** ***(st dev ±1 min)*** | **pH after crosslinking** ***(st dev ±0.1)*** |
|---|---|---|---|---|
| Pect M-HA | pH 3.2 | M-HA | < 4 | 3.5 |
| | pH 3.7 | | > 60 | 4.2 |
| Pect m-HA | pH 3.2 | m-HA | < 4 | 3.4 |
| | pH 3.7 | | < 4 | 4.7 |
| Pect n-HA $_{(RT)}$ | pH 3.2 | n-HA $_{(RT)}$ | < 4 | 3.4 |
| | pH 3.7 | | 5 | 4.1 |
| Pect n-HA $_{(650°C)}$ | pH 3.2 | n-HA $_{(650°C)}$ | < 4 | 3.4 |
| | pH 3.7 | | 8 | 4.2 |

*Table 3. COO-R/COO⁻ Peak area ratio of the produced pectin-hydroxyapatite hydrogels*

| | ***Peak areas (normalized to the area of the CH stretching at 2940 $cm^{-1}$)*** | | | ***(COOH + COO-R)/COO⁻ ratio*** |
|---|---|---|---|---|
| | *1745 $cm^{-1}$* | *1625 $cm^{-1}$* | *1420 $cm^{-1}$* | *1745 $cm^{-1}$/ (1625 $cm^{-1}$ +1420 $cm^{-1}$)* |
| Pect n-HA pH 3.2 | 1.71 | 8.97 | 0.13 | 0.19 |
| Pect n-HA pH 3.7 | 1.48 | 11.48 | 0.19 | 0.13 |
| Pect m-HA pH 3.2 | 9.22 | 38.38 | 2.00 | 0.23 |
| Pect m-HA pH 3.7 | 1.5 | 11.24 | 0.22 | 0.13 |
| Pect M-HA pH 3.2 | 2.60 | 8.16 | 0.15 | 0.31 |
| Pect M-HA pH 3.7 | 0.81 | 5.24 | 0.04 | 0.15 |
| Pectin powder (reference) | 2.66 | 3.70 | 0.04 | 0.71 |

**Figure captions**

Figure 1. SEM micrographs of (a) M-HA, (b) m-HA, (c) n-$HA_{(RT)}$ and (d) n-$HA_{(650°C)}$ powders.

Figure 2. TEM micrograph of n-HA powders: (a) as produced and (b) calcined at 650°C.

Figure 3. Particle size distribution (fractional and cumulative) for n-$HA_{(650°C)}$ powders by TEM analysis.

Figure 4. XRD diagrams of the considered HA powders; the standard reflexes for pure hydroxyapatite ($Ca_5(PO_4)_3OH$ - JCPDS No: 09-0432) are shown for comparison

Figure 5. FTIR spectra of (a) n-$HA_{(RT)}$ and n-$HA_{(650°C)}$ and (b) comparison among the FTIR spectra of calcined n-HA, m-HA and M-HA.

Figure 6. $^{31}P$ CP MAS NMR spectra of n-$HA_{(RT)}$ and n-$HA_{(650°C)}$ (a) and $^{1}H$ MAS NMR spectra of n-$HA_{(RT)}$ and n-$HA_{(650°C)}$ (b).

Figure 7. $N_2$ adsorption-desorption isotherms of (a) as-prepared n-$HA_{(RT)}$ and (b) 650°C heated n-$HA_{(650°C)}$ powders. BJH pore size distribution of (c) n-$HA_{(RT)}$ and (d) n-$HA_{(650°C)}$ powders.

Figure 8. ICP analyses on hydroxyapatite powders at pH 3.2, 3.7 and 7 and at different incubation times (10 min and 24h).

Figure 9. SEM micrographs of (a) Pect M-HA, (b) Pect m-HA and (c) Pect n-$HA_{650°C}$ composites.

Figure 10. FTIR spectra of (a) Pect M-HA, (b) Pect m-HA and (c) Pect n-$HA_{650°C}$ composite pectin-hydroxyapatite hydrogels.

Figure 11. Rheological characterization of pectin- hydroxyapatite hydrogels: (a) complex viscosity and (b) storage modulus of the hydrogels as function of frequency. Comparison of the storage modulus of as-prepared and calcined n-HA hydrogels (c).

Figure 12. Temperature ramp analyses of the produced hydrogels (a) and comparison of the temperature-dependent behavior of n-$HA_{RT}$ and n-$HA_{650°C}$ hydrogels (b).

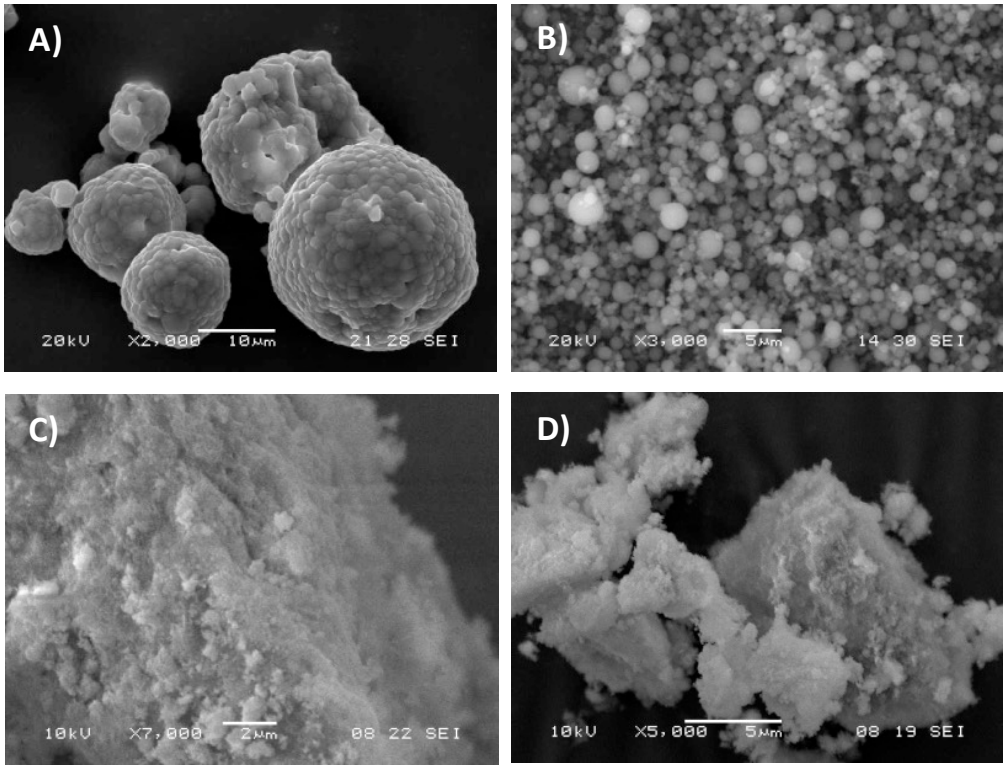


Figure 1

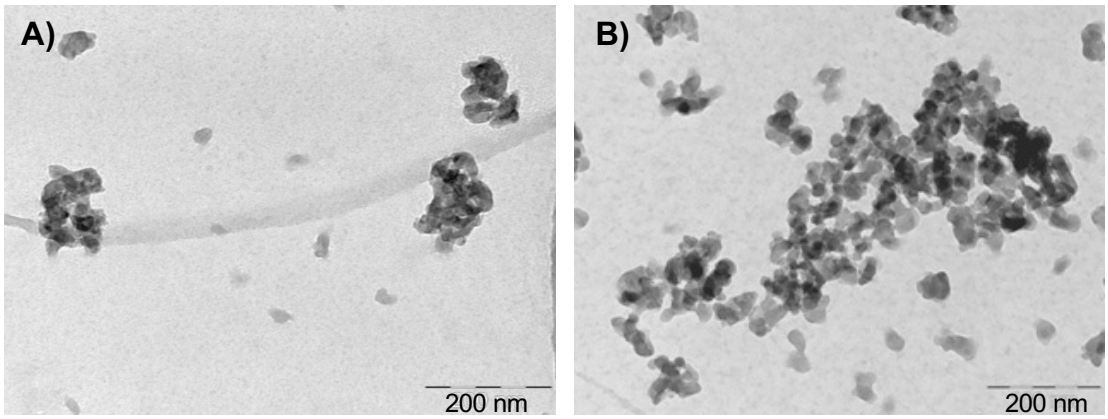


Figure 2

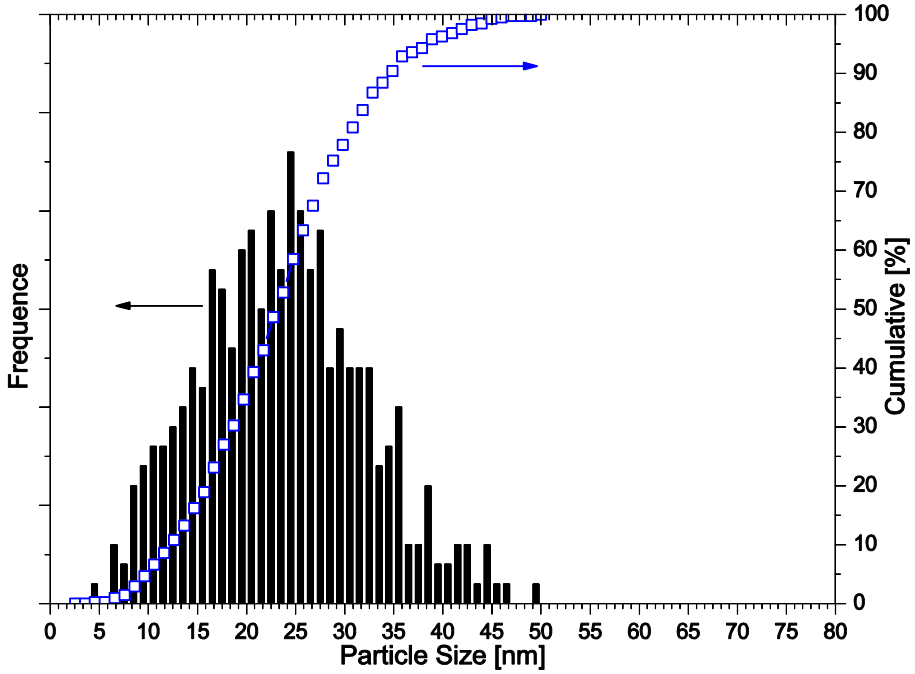


Figure 3

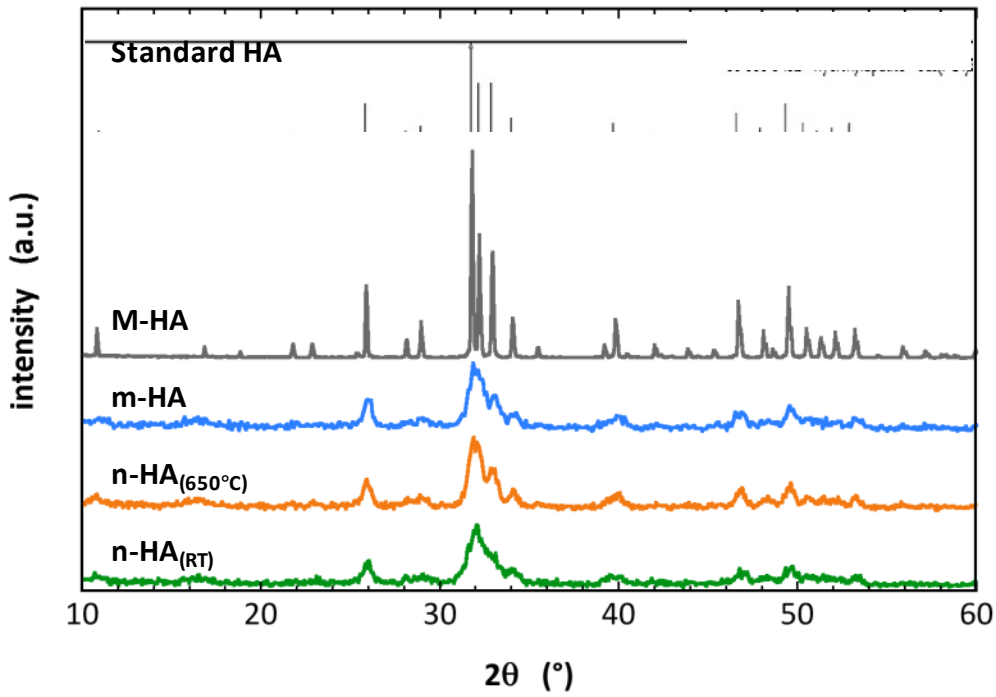


Figure 4

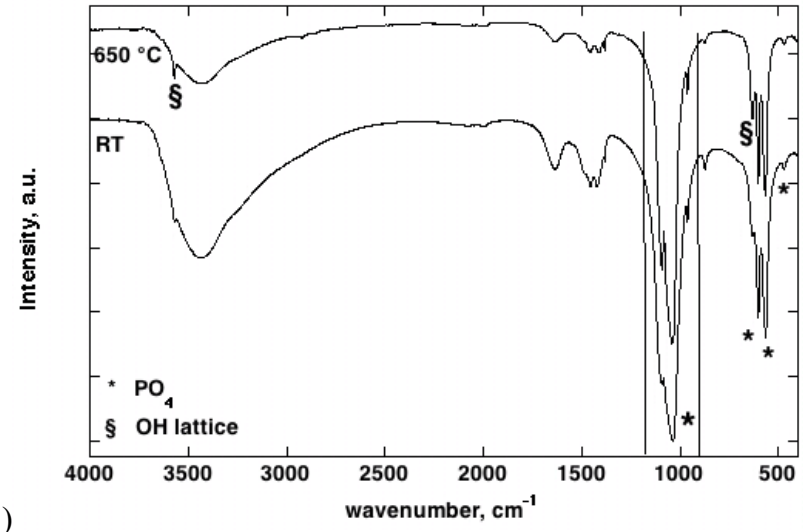


)

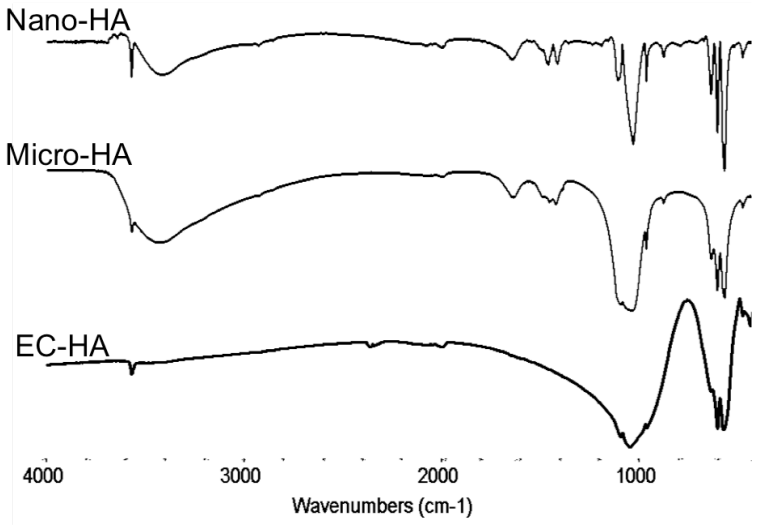


B)

Figure 5

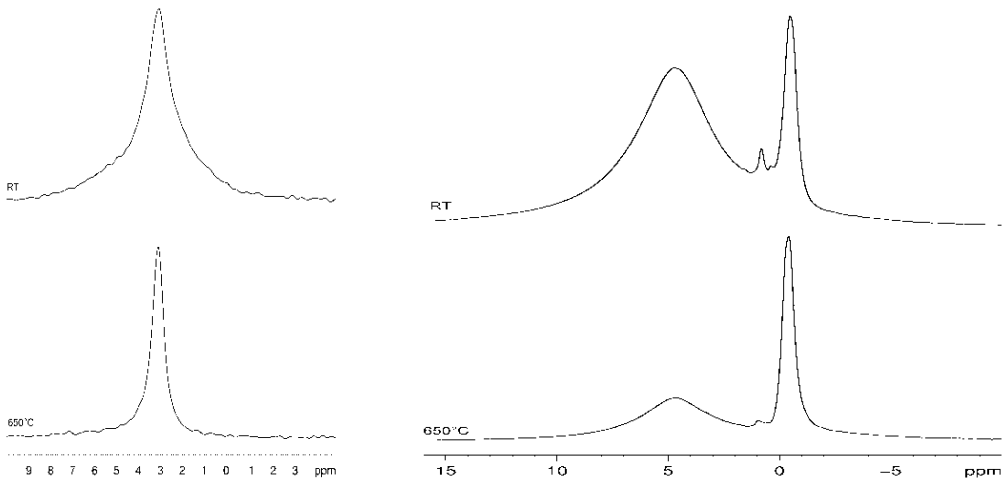


a) b)

Figure 6

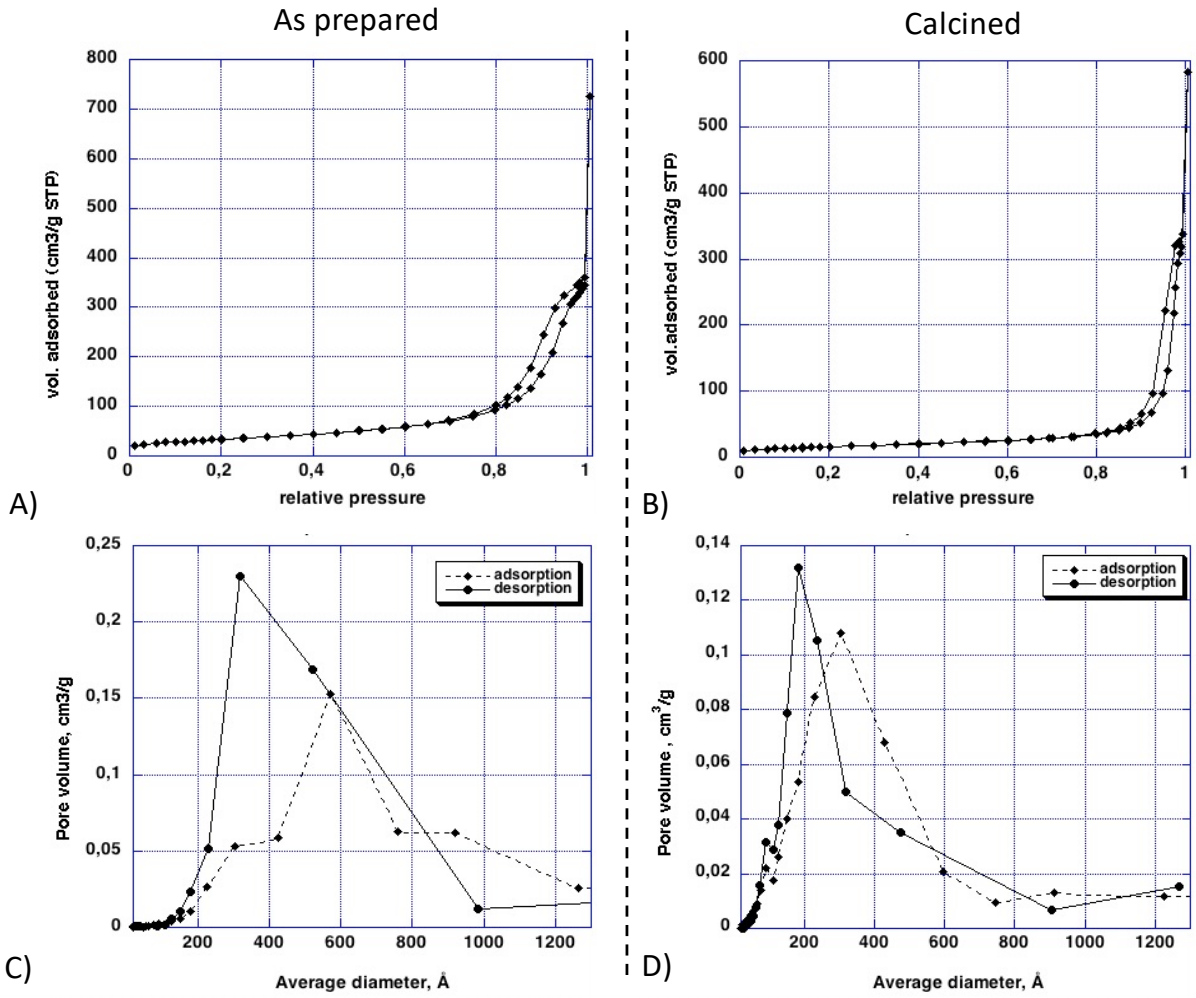
As prepared
Calcined
A)
B)
C)
D)
vol. adsorbed (cm3/g STP)
vol.adsorbed (cm3/g STP)
relative pressure
Pore volume, cm3/g
Pore volume , cm3/g
Average diameter, Å
adsorption
desorption

Figure 7

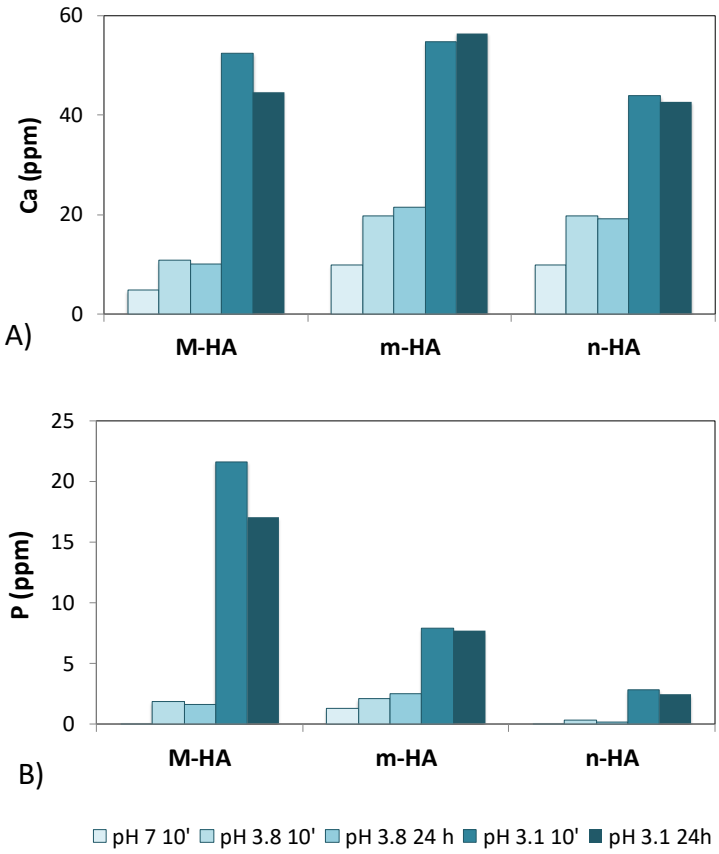


Figure 8

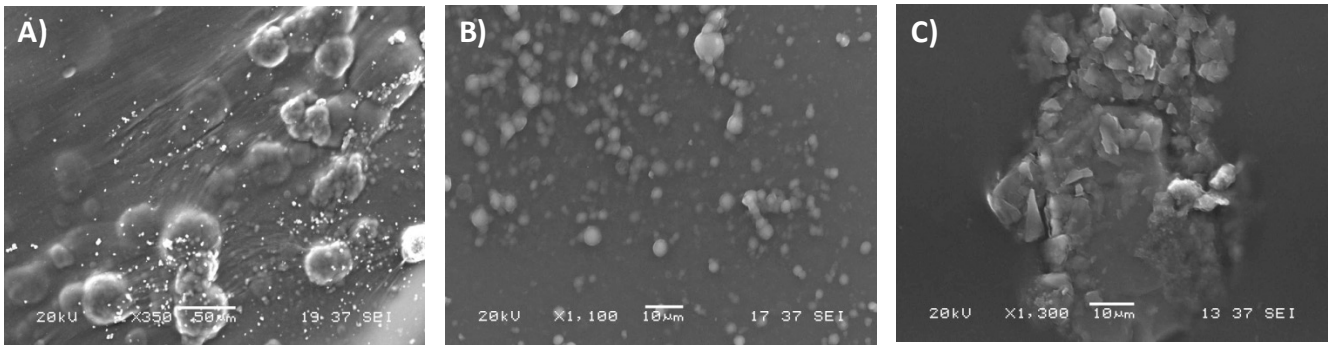


Figure 9

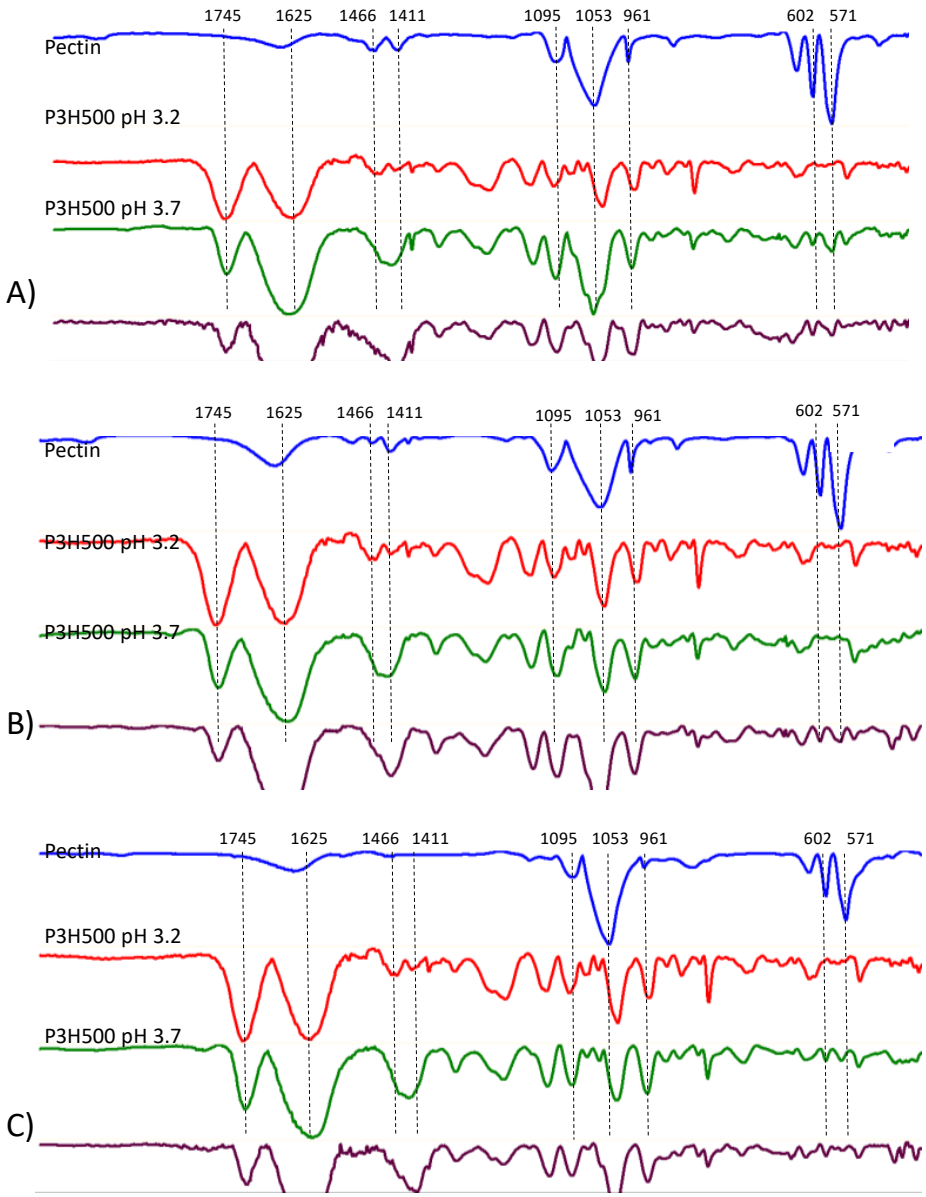
1745
1625
1466
1411
1095
1053
961
602
571
Pectin
P3H500 pH 3.2
P3H500 pH 3.7
A)
B)
C)

Figure 10

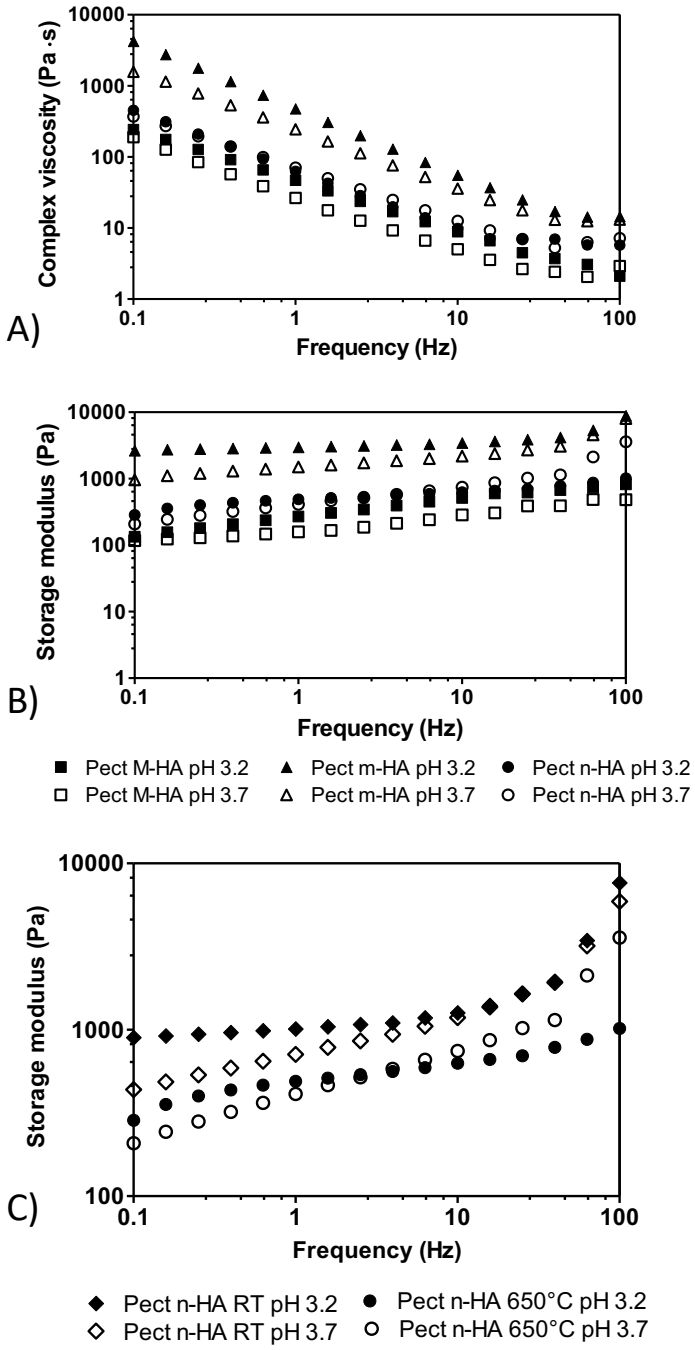
A)
Complex viscosity (Pa·s)
10000
1000
100
10
1
0.1
1
10
100
Frequency (Hz)
B)
Storage modulus (Pa)
10000
1000
100
10
1
0.1
1
10
100
Frequency (Hz)
Pect M-HA pH 3.2
Pect m-HA pH 3.2
Pect n-HA pH 3.2
Pect M-HA pH 3.7
Pect m-HA pH 3.7
Pect n-HA pH 3.7
C)
Storage modulus (Pa)
10000
1000
100
0.1
1
10
100
Frequency (Hz)
Pect n-HA RT pH 3.2
Pect n-HA 650°C pH 3.2
Pect n-HA RT pH 3.7
Pect n-HA 650°C pH 3.7

Figure 11

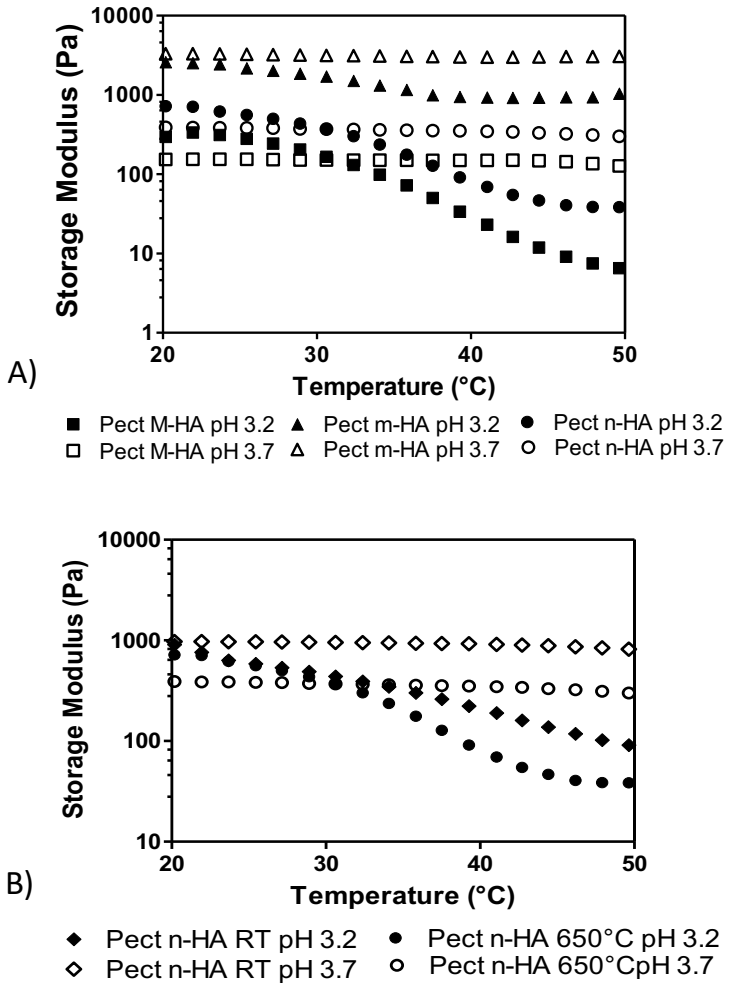
A)
Storage Modulus (Pa)
10000
1000
100
10
1
20
30
40
50
Temperature (°C)
Pect M-HA pH 3.2
Pect m-HA pH 3.2
Pect n-HA pH 3.2
Pect M-HA pH 3.7
Pect m-HA pH 3.7
Pect n-HA pH 3.7
B)
Storage Modulus (Pa)
10000
1000
100
10
20
30
40
50
Temperature (°C)
Pect n-HA RT pH 3.2
Pect n-HA 650°C pH 3.2
Pect n-HA RT pH 3.7
Pect n-HA 650°CpH 3.7

Figure 12